



Short communication

Electrochemical performance of mixed valence $\text{Na}_3\text{V}_2\text{O}_{2x}(\text{PO}_4)_2\text{F}_{3-2x}/\text{C}$ as cathode for sodium-ion batteriesPaula Serras ^a, Verónica Palomares ^a, Aitzane Goñi ^a, Pierre Kubiak ^b, Teófilo Rojo ^{a,b,*}^a Departamento de Química Inorgánica, Universidad del País Vasco UPV/EHU, P.O. Box 644, 48080 Bilbao, Spain^b CIC ENERGIGUNE, Parque Tecnológico de Álava, Albert Einstein 48, ED. CIC, 01510 Miñano, Spain

HIGHLIGHTS

- Simple synthesis of mixed valence $\text{Na}_3\text{V}_2\text{O}_{2x}(\text{PO}_4)_2\text{F}_{3-2x}/\text{C}$ composite ($0 < x < 1$).
- Composite electrodes operate at 3.6–4.1 V vs. Na/Na^+ with high specific capacity (100 mAh g^{-1} at C/20).
- Composite electrodes show excellent rate capability for charging rates up to 5C (75 mAh g^{-1}).
- Superior reversibility and stability are observed for 200 cycles at 1C (95 mAh g^{-1}).

ARTICLE INFO

Article history:

Received 9 January 2013

Received in revised form

11 April 2013

Accepted 19 April 2013

Available online 29 April 2013

Keywords:

Na-ion batteries

Electrochemistry

Mixed-valence

Sodium vanadium fluorophosphates

ABSTRACT

A composite made of a mixed-valence sodium–vanadium fluorophosphate and 6.4% wt. carbon, $\text{Na}_3\text{V}_2\text{O}_{2x}(\text{PO}_4)_2\text{F}_{3-2x}/\text{C}$ ($0 < x < 1$), has been prepared. Structural and magnetic characterization confirmed the +3/+4 oxidation state of vanadium in the phase. Morphological and texture analyses showed that carbon forms a network surrounding the particles, leading to a mesoporous composite with a high specific area of $67 \text{ m}^2 \text{ g}^{-1}$. Electrochemical characterization conducted in Swagelok cells by cyclic voltammetry and galvanostatic cycling indicated that sodium extraction/insertion proceeds through a complex mechanism in two voltage *pseudo-plateaus* at 3.6 and 4.1 V vs. Na/Na^+ . Rate capability of the material ranges from specific capacities of 100 mAh g^{-1} at C/20 to 75 mAh g^{-1} at 5C. Cycling stability at 1C showed coulombic efficiency higher than 99% and capacity retention of 95% after 200 cycles.

© 2013 Elsevier B.V. All rights reserved.

1. Introduction

Na-ion batteries have turned up in the last year as a solid alternative or complement to Li-ion battery technology due to the natural abundance of sodium, its low price and similar intercalation chemistry to lithium [1,2]. This way, works in the field of battery materials have been extended to Na-based intercalation compounds. The main issue of Na-ion based systems is their lower energy density compared to Li-ion and the smaller choice of electrode materials available for the sodium technology. Among the possible cathode materials, sodium–vanadium phosphates and fluorophosphates show very interesting electrochemical performance. First, the inductive effects of both PO_4^{3-} and F^- anions allow a high working potential [3] and second, a high specific capacity can be expected due to the multiple accessible oxidation states of vanadium. Thus,

materials such as $\text{Na}_3\text{V}_2(\text{PO}_4)_3$ [4], $\text{Na}_3\text{V}_2(\text{PO}_4)_2\text{F}_3$ [5,6] and $\text{Na}_3(\text{VO})_2(\text{PO}_4)_2\text{F}$ [7] show good charge/discharge capacity and good cyclability and, therefore, they can be considered as interesting cathode materials for Na-ion batteries. A family of compounds with the general formula: $\text{Na}_3\text{V}_2\text{O}_{2x}(\text{PO}_4)_2\text{F}_{3-2x}$ where the $\text{V}^{3+}/\text{V}^{4+}$ ratio is linked to the fluorine content has been recently published. The materials were prepared using a carbon containing ceramic V^{3+} composite precursor (VPO_4) and sodium fluorine in hydrothermal conditions [8]. Carbon contained in VPO_4 precursor plays a protective role in this reaction, avoiding the complete oxidation of V^{3+} to V^{4+} in the autoclave during hydrothermal treatment. The resulting mixed-valence material presents good electrochemical performance with high working potential (*plateaus* at 3.6 and 4.1 V vs. Na/Na^+), good specific capacity and cycling stability. Moreover, this family of compounds presents a maximum energy density value of 0.533 Wh g^{-1} , that is the highest among other phosphate compounds proposed as cathodes for Na-ion batteries [8].

In addition to the intrinsic electrochemical properties due to composition, morphological properties of the materials play a role

* Corresponding author. Tel.: +34 946012458; fax: +34 946013500.

E-mail addresses: teo.rojo@ehu.es, troj@cicenergigune.com (T. Rojo).

on their electrochemical performance. For Li insertion materials, nanosized electrodes have shown improved electrochemical behaviour when compared to bulk materials [9–12]. Small crystallite size of nanosized materials leads to faster lithium insertion/extraction together with a large specific surface area that provides a greater electrode/electrolyte interface. In this context, mesoporous materials have received particular attention since they are demonstrated to present an optimal morphology for electrode stability and Li insertion capacity, especially at high charge/discharge rates [13–15]. Similarly to the Li intercalation materials, it can be expected that the morphology strongly influences the electrochemical performance of the Na insertion materials.

In the present work, we investigate the electrochemical behaviour of a mesoporous mixed valence $\text{Na}_3\text{V}_2\text{O}_{2x}(\text{PO}_4)_2\text{F}_{3-2x}/\text{C}$ material prepared in hydrothermal conditions. This material shows excellent electrochemical performance in terms of capacity, cyclability, stability and reversibility, especially at high charge/discharge rates.

2. Experimental

2.1. Sample preparation

A sample of the $\text{Na}_3\text{V}_2\text{O}_{2x}(\text{PO}_4)_2\text{F}_{3-2x}$ compound was synthesized by hydrothermal method from a ceramic precursor. Thus, the synthesis process took place in two steps. First, VPO_4/C composite was synthesized by the ceramic method. For this purpose, V_2O_5 (Sigma–Aldrich, 99.99% purity) and $\text{NH}_4\text{H}_2\text{PO}_4$ (Fluka, 99.5% purity) were mixed in an agate mortar in stoichiometric ratio with a 25% molar excess of Kejten black. This mixture was annealed twice under nitrogen atmosphere at 300 and 850 °C. Second, sodium fluorophosphate sample was prepared under mild hydrothermal conditions and autogenous pressure (10–20 bar at 170 °C) by reacting NaF (Sigma–Aldrich, 99% purity) and VPO_4/C in 3.3/1 molar proportion. The reaction mixture was sealed in a polytetrafluoroethylene (PTFE)-lined steel pressure vessel, which was maintained at 170 °C for 65 h.

2.2. Structural characterization

Elemental analysis was performed in a Eurovector 3000 equipment. Powder diffraction patterns were collected in a Bruker D8 Advance Vário diffractometer working with $\text{Cu K}-\alpha$ radiation at room temperature. The morphological characterization was made by Scanning Electron Microscopy (SEM) in a JEOL JSM-7000F microscope equipped with Energy Dispersive X-ray Analysis (EDX). Specific surface area of the mesoporous samples was measured by nitrogen sorption with an ASAP2020 instrument (Micromeritics) and calculated based on the Brunauer–Emmet–Teller (BET) equation in the relative pressure (p/p_0) range of 0.05–0.3. The pore size distribution was determined according to Barrett, Joyner and Halenda (BJH) from the desorption branch of the isotherm.

2.3. Electrochemical characterization

The positive electrodes were manufactured by mixing 80% wt. carbon coated $\text{Na}_3\text{V}_2\text{O}_{2x}(\text{PO}_4)_2\text{F}_{3-2x}$ active material, 10% wt. conductive carbon (Super C65, Timcal) and 10% wt. polyvinylidene-fluoride binder (PVDF 5130, Solvay). A few mL N-methylpyrrolidone (NMP) (Aldrich) were added and the resulting slurry was stirred for 1 h. The resulting slurry was coated on an aluminium foil using “doctor blade” technique. The electrode film was dried at 80 °C in a vacuum oven for 24 h. Circular electrodes were cut from the foil, pressed for better contact of the coated material and aluminium current collector, dried (120 °C) under vacuum overnight and finally

transferred in an argon filled glove box (Jacomex). The mass loading of the electrodes was 3 mg cm^{-2} approximately. $\text{Na}/(\text{Na}_3\text{V}_2\text{O}_{2x}(\text{PO}_4)_2\text{F}_{3-2x}/\text{C})$ half-cells consisted of a working electrode ($\text{Na}_3\text{V}_2\text{O}_{2x}(\text{PO}_4)_2\text{F}_{3-2x}$), a counter electrode (sodium metal), a glass microfiber separator (Whatman, GF/A) and a 1 M NaPF_6 EC:DMC (1:1 by wt%) with 2% FEC additive (mono-fluoroethylene carbonate) electrolyte. The electrochemical evaluation of the samples was made by galvanostatic cycling and cyclic voltammetry with a Biologic VMP3 Multi-channel potentiostat-galvanostat. Cyclic voltammetry was carried out for $\text{Na}/(\text{Na}_3\text{V}_2\text{O}_{2x}(\text{PO}_4)_2\text{F}_{3-2x}/\text{C})$ half-cells between 2.8 and 4.3 V vs. Na/Na^+ at scan rates ranging from 0.1 mV s^{-1} to 1 mV s^{-1} . Galvanostatic cycling was performed for $\text{Na}/(\text{Na}_3\text{V}_2\text{O}_{2x}(\text{PO}_4)_2\text{F}_{3-2x}/\text{C})$ half-cells between 2.8 and 4.3 V vs. Na/Na^+ at rates ranging from C/20 to 5C. All potentials mentioned in this study are given vs. Na/Na^+ . The maximum Na extraction from $\text{Na}_3\text{V}_2\text{O}_{2x}(\text{PO}_4)_2\text{F}_{3-2x}$ was assumed to be 2 (130 mAh g^{-1}), and thus the charging rates in the measurements were based on the following relationship: 1C = 130 mA g^{-1} .

3. Results and discussion

3.1. Material characterization

The $\text{Na}_3\text{V}_2\text{O}_{2x}(\text{PO}_4)_2\text{F}_{3-2x}$ compound is prepared by hydrothermal method from a carbon containing VPO_4 ceramic precursor. The black colour of the obtained powder suggests that some carbon is still present in the material and indeed the elemental analysis shows that a 6.4% wt. of carbon remains in the final product. The sample was examined by XRD, showing well-defined diffraction maxima, and thus, good crystallinity. As it can be seen in Fig. 1, the diffraction peaks were indexed to a main phase with $\text{P}4_2/\text{mm}$ space group and the following cell parameters: $a = 9.030(3)$ Å and $c = 10.644(7)$ Å, that are intermediate between the extreme compositions of this family: $\text{Na}_3(\text{VO})_2(\text{PO}_4)_2\text{F}$ phase ($x = 1$; $a = 9.03051(2)$ Å, $c = 10.62002(3)$ Å [16]) and $\text{Na}_3\text{V}_2(\text{PO}_4)_2\text{F}_3$ ($x = 0$; $a = 9.047(2)$ Å, $c = 10.705(2)$ Å [17]). These phases posses the same structure and are the extremes of a family of compounds with general formula $\text{Na}_3\text{V}_2\text{O}_{2x}(\text{PO}_4)_2\text{F}_{3-2x}$ ($0 < x < 1$) where one F is replaced by an O atom. This way, vanadium oxidation state varies from V^{3+} to V^{4+} as fluorine decreases and oxygen increases [8]. A small amount of unreacted VPO_4 initial precursor was also observed in the diffractogram.

The formation of the $\text{V}^{3+}/\text{V}^{4+}$ mixed valence phase is attributed to the presence of carbon in the synthesis process which prevents the complete oxidation from V^{3+} to V^{4+} during the hydrothermal

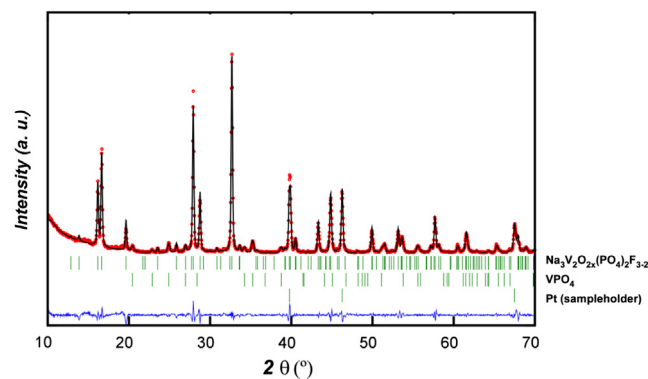


Fig. 1. Pattern matching of XRD diagram of the material before electrochemical tests. Experimental (red circles), fitted (black line) and difference between them (blue lower line). (For interpretation of the references to colour in this figure legend, the reader is referred to the web version of this article.)

treatment. In addition to its protective role against oxidation, the carbon also influences the morphology of the final composite material. Fig. 2 shows SEM images of the carbon containing $\text{Na}_3\text{V}_2\text{O}_{2x}(\text{PO}_4)_2\text{F}_{3-2x}$. The material is made of homogeneous agglomerates of several micrometres (Fig. 2a). EDX analysis of two zones of the material (Table 1) indicated that the grains of about 1 μm size (point 1) posses the element ratio corresponding to the sodium-vanadium fluorophosphate with a minimum presence of carbon. However, the analysis on an agglomerate (point 2) showed a much larger proportion of carbon apart from the expected element ratio for the studied compound.

These data show that the agglomerates are composed of primary particles of about 1 μm size embedded in a carbon matrix distributed all over the material. This way, the carbon introduced in the synthesis process creates an intimate contact between the electrode material and the carbon which can be beneficial for enhanced electrochemical performance (Fig. 2b). Moreover, the synthesis method leads to the formation of a porous composite material $\text{Na}_3\text{V}_2\text{O}_{2x}(\text{PO}_4)_2\text{F}_{3-2x}/\text{C}$ that presents a specific surface area of $67 \text{ m}^2 \text{ g}^{-1}$. The isotherm shown in Fig. 3 can be classified as type IV according to the classification given by Brunauer et al. [19]. The hysteresis H2 of this isotherm type is characteristic of mesoporous materials with drop shaped pores. The pore size distribution was obtained using the BJH (Barrett, Joyner & Halenda) method from the adsorption isotherm. The $\text{Na}_3\text{V}_2\text{O}_{2x}(\text{PO}_4)_2\text{F}_{3-2x}/\text{C}$ sample

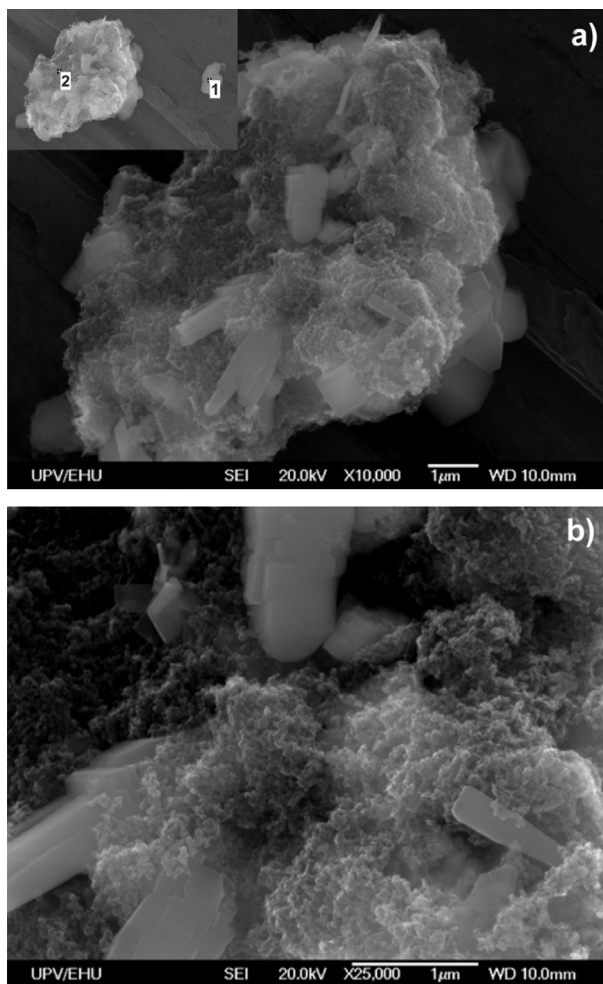


Fig. 2. SEM images of the sample a) 5000 \times , b) 10000 \times and c) 25000 \times . Connectivity between particles established by small size granules is shown with arrows.

Table 1
Ratio of the different elements found by EDX in the SEM analysis.

| | Atomic ratio between elements | | | | |
|---------|-------------------------------|---|---|-----|------|
| | Na | V | P | F | C |
| Point 1 | 1.3 | 1 | 1 | 1.6 | 1.7 |
| Point 2 | 1.5 | 1 | 1 | 2.6 | 43.3 |

exhibits a narrow pore size distribution with a maximum at 3.6 nm (Fig. 3 inset). From the SEM micrographs, it can be deduced that the porosity of the composite material is essentially due to the arrangement between $\text{Na}_3\text{V}_2\text{O}_{2x}(\text{PO}_4)_2\text{F}_{3-2x}$ particles and the carbon.

The synthesis method used in this work to prepare the $\text{Na}_3\text{V}_2\text{O}_{2x}(\text{PO}_4)_2\text{F}_{3-2x}/\text{C}$ composite leads to a good control of the chemical composition, structure and morphology of the material. It is worth noting the triple role of the carbon in the preparation of the material. First, it prevents the complete oxidation of V^{3+} to V^{4+} during the hydrothermal process. Second, it induces the formation of a mesoporous composite which generally leads to a better contact between electrode material/electrolyte in electrochemical cells. Finally, the presence of carbon in the final material as electronic conductor avoids further carbon coating treatment.

3.2. Electrochemical evaluation

The electrochemical behaviour of the $\text{Na}_3\text{V}_2\text{O}_{2x}(\text{PO}_4)_2\text{F}_{3-2x}/\text{C}$ composite is investigated by both cyclic voltammetry and galvanostatic cycling. Cyclic voltammetry is carried out between 2.8 and 4.3 V vs. Na/Na^+ at scan rates ranging from 0.1 mV s^{-1} to 1 mV s^{-1} . The comparison between the voltammograms is shown in Fig. 4. The voltammograms present two pairs of peaks at about 3.75 V and 4.1 V (anodic) and 3.45 V and 4.0 V (cathodic) corresponding to the faradaic extraction/insertion of sodium from/into $\text{Na}_3\text{V}_2\text{O}_{2x}(\text{PO}_4)_2\text{F}_{3-2x}/\text{C}$. The values of the redox potentials agree with those reported in the literature [7,8,18]. At low scan rate (0.1 mV s^{-1}) the broadness of the redox peaks indicates complex electrochemical mechanisms. Chihara et al. [5] and Shakoor et al., [18] have investigated the electrochemical mechanism of the reversible Na extraction from the $\text{Na}_3\text{V}_2(\text{PO}_4)_2\text{F}_3$ material. Both groups reported

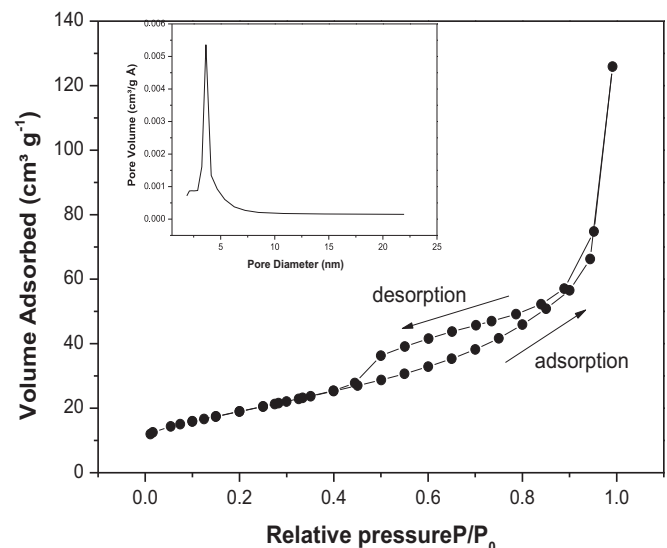


Fig. 3. N_2 adsorption–desorption isotherms of carbon coated $\text{Na}_3\text{V}_2\text{O}_{2x}(\text{PO}_4)_2\text{F}_{3-2x}$ and BJH pore size distribution (inset).

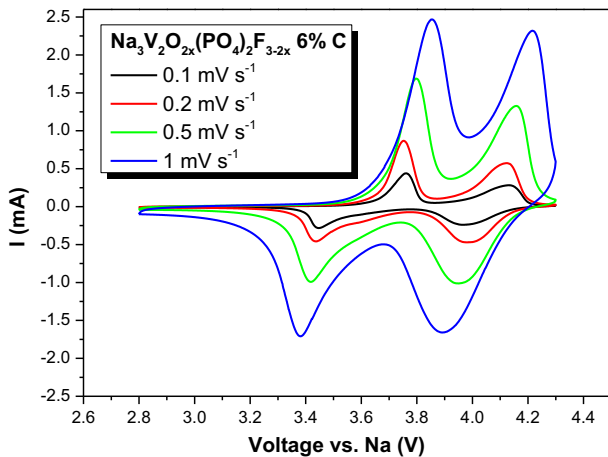


Fig. 4. Cyclic voltammetry of $\text{Na}_3\text{V}_2\text{O}_{2x}(\text{PO}_4)_2\text{F}_{3-2x}$ at scan rates from 0.1 mV s^{-1} to 1 mV s^{-1} .

that the electrochemical reaction occurs through a single-phase reaction with negligible ($\sim 2\%$) volume variation. Similar single-phase mechanism is expected for the $\text{Na}_3\text{V}_2\text{O}_{2x}(\text{PO}_4)_2\text{F}_{3-2x}/\text{C}$ mixed valence material which can explain the shape of the redox peaks observed in the cyclic voltammograms. By increasing the

scan rate from 0.1 to 1 mV s^{-1} it can be observed that the anodic (extraction) potential shifts to higher voltages and the cathodic (insertion) potential shifts to lower voltages. This is due to the increased polarization at higher sweep rates because of kinetic limitations associated with the sodium diffusion through the active material. However, the potential shifts are moderate, which suggests the existence of fast kinetics and rapid storage mechanism for $\text{Na}_3\text{V}_2\text{O}_{2x}(\text{PO}_4)_2\text{F}_{3-2x}$. A typical charge–discharge curve ($\text{C}/20$) of the composite is shown in Fig. 5. The electrochemical charge presents two pseudo-plateaus of similar length at 3.6 and 4.1 V vs. Na⁺. The specific capacity measured at $\text{C}/20$ is about 100 mA h g^{-1} which corresponds to $\sim 80\%$ of the theoretical capacity, equally distributed among the lower (3.6 V) and the higher potential (4.1 V). A qualitative evaluation of the mechanism can be done by derivation of the galvanostatic curves. From the dQ/dV curve (Fig. 5b), it appears that the mechanism of Na extraction/insertion from/into $\text{Na}_3\text{V}_2\text{O}_{2x}(\text{PO}_4)_2\text{F}_{3-2x}$ is not easy to describe and involves complex processes. A deeper study of the Na extraction/insertion mechanism is currently in progress.

Rate capabilities of $\text{Na}_3\text{V}_2\text{O}_{2x}(\text{PO}_4)_2\text{F}_{3-2x}/\text{C}$ at charging rates ranging from $\text{C}/20$ to 5 C between 2.8 and 4.3 V are shown in Fig. 6. The specific capacity shows excellent values for charging rates up to 5 C . Indeed, the measured specific capacity is 100 mA h g^{-1} at a rate of $\text{C}/20$. This value decreases to 99 mA h g^{-1} at $\text{C}/10$, 98 mA h g^{-1} at $\text{C}/5$, 95 mA h g^{-1} at $\text{C}/2$, 91 mA h g^{-1} at C , 86 mA h g^{-1} at 2 C , and finally, 75 mA h g^{-1} at 5 C . A low coulombic efficiency is observed in the first cycles, however, for the first cycle at $\text{C}/20$ the coulombic

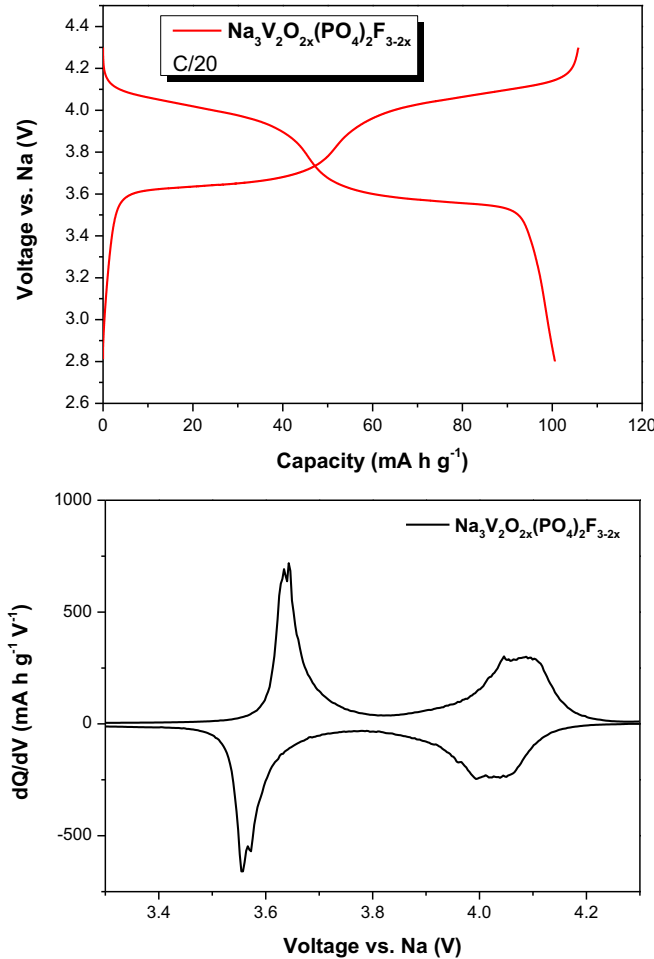


Fig. 5. Typical galvanostatic Na⁺ extraction/insertion curves from/into $\text{Na}_3\text{V}_2\text{O}_{2x}(\text{PO}_4)_2\text{F}_{3-2x}$ and corresponding dQ/dV curve.

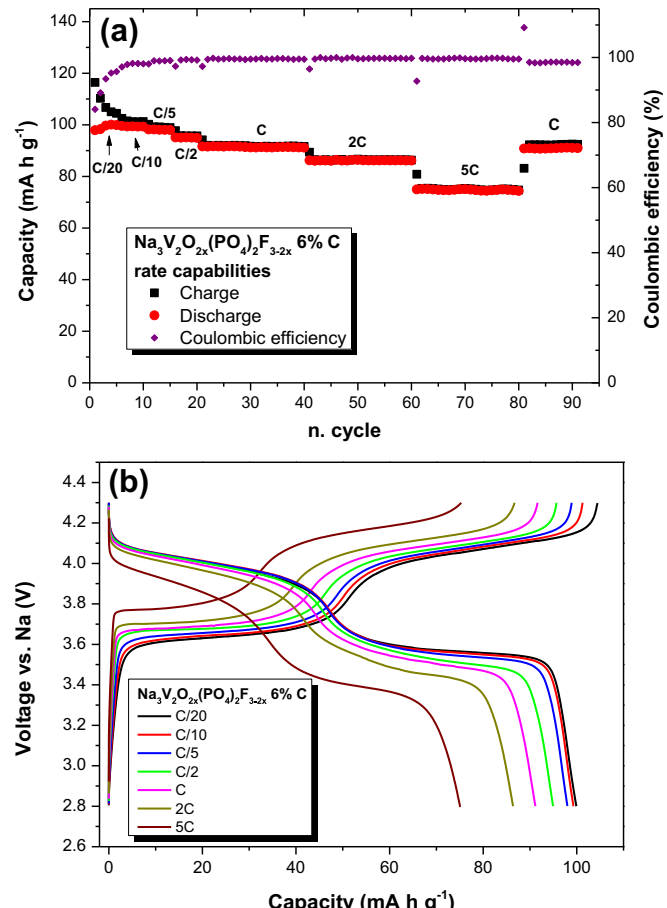


Fig. 6. (a) Specific charge/discharge capacity of $\text{Na}_3\text{V}_2\text{O}_{2x}(\text{PO}_4)_2\text{F}_{3-2x}$ at different C rates and (b) typical galvanostatic Na⁺ extraction/insertion curves from/into $\text{Na}_3\text{V}_2\text{O}_{2x}(\text{PO}_4)_2\text{F}_{3-2x}$ at different charging rates from $\text{C}/20$ to 5C .

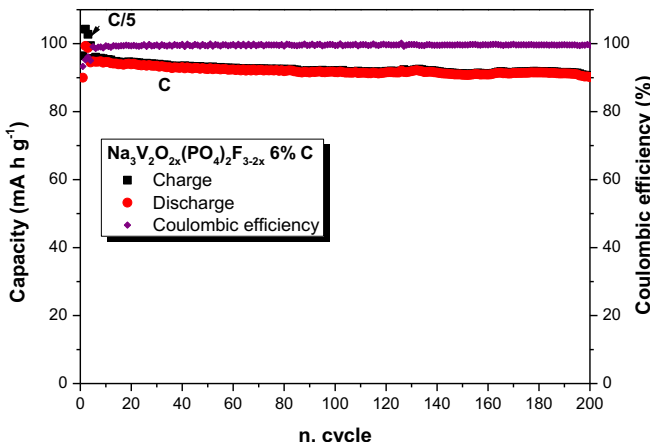


Fig. 7. Cycling stability of $\text{Na}_3\text{V}_2\text{O}_{2x}(\text{PO}_4)_2\text{F}_{3-2x}$ over 200 cycles with a charge/discharge rate of C. The first 3 cycles were recorded with C/5.

efficiency is only 83% and it progressively increases to 95% after 5 cycles becoming higher than 99% after 15 cycles. The voltage profile and the discharge/charge capacity evolution of $\text{Na}_3\text{V}_2\text{O}_{2x}(\text{PO}_4)_2\text{F}_{3-2x}/\text{C}$ at increasing current from C/20 to 5 C are presented in Fig. 6b. A small increase of the polarization is observed with increasing current. The cycling stability has been evaluated by repetitive charge–discharge at 1 C rate for 200 cycles. Prior to the cycling, measurement at lower rate has been carried out in order to stabilize the Na metal anode. The evolution of the capacity upon cycling is given in Fig. 7. As it can be seen, the $\text{Na}_3\text{V}_2\text{O}_{2x}(\text{PO}_4)_2\text{F}_{3-2x}/\text{C}$ composite exhibits an excellent cycling stability. The C rate capacity is 95 mA h g^{−1} at the beginning of the cycling and 90 mA h g^{−1} with a coulombic efficiency >99% after 200 cycles which corresponds to 95% capacity retention.

Finally, the $\text{Na}_3\text{V}_2\text{O}_{2x}(\text{PO}_4)_2\text{F}_{3-2x}/\text{C}$ material exhibits high capacities, rate capabilities, reversibility and stability upon cycling. These features make $\text{Na}_3\text{V}_2\text{O}_{2x}(\text{PO}_4)_2\text{F}_{3-2x}/\text{C}$ a very promising cathode for Na-ion batteries.

4. Conclusions

This work shows the electrochemical performance of a mesoporous carbon-containing $\text{Na}_3\text{V}_2\text{O}_{2x}(\text{PO}_4)_2\text{F}_{3-2x}/\text{C}$ composite. This material is prepared by a simple synthesis process that leads to the presence of carbon in the final product. Carbon generated during the synthesis process has a great influence on the material. First, it generates the mixed valence, by avoiding the complete oxidation of V^{3+} to V^{4+} during hydrothermal process. Second, it forms a porous conductive network around the active material particles, which

allows better access of liquid electrolyte and electrons to the active material. These two features enhance the electrochemical performance of the sodium–vanadium fluorophosphate material. This way, the $\text{Na}_3\text{V}_2\text{O}_{2x}(\text{PO}_4)_2\text{F}_{3-2x}/\text{C}$ composite demonstrates to operate at high voltages vs. Na/Na^+ with excellent rate capability for charging rates up to 5C and superior reversibility and stability for 200 cycles at 1C, which makes this material a high quality cathode for Na-ion batteries.

Acknowledgements

This work was financially supported by the Ministerio de Educación y Ciencia (MAT2010-19442), the Universidad del País Vasco/Euskal Herriko Unibertsitatea (GIU06-11) and the Gobierno Vasco/Eusko Jaurlaritza (Etortek CIC Energigune 10 and SAIOTEK-12 ENERGIBA). The authors would like to thank Dr. Julie Segalini for the nitrogen -sorption measurements.

References

- [1] V. Palomares, P. Serras, I. Villaluenga, K.B. Hueso, J. Carretero-Gonzalez, T. Rojo, *Energy Environ. Sci.* 5 (2012) 5884–5901.
- [2] S.-W. Kim, D.-H. Seo, X. Ma, G. Ceder, K. Kang, *Adv. Energy Mater.* 2 (2012) 710–721.
- [3] A. Yamada, S.C. Chung, K. Hinokuma, *J. Electrochem. Soc.* 148 (2001) A224–A229.
- [4] Z. Jian, L. Zhao, H. Pan, Y.-S. Hu, H. Li, W. Chen, L. Chen, *Electrochim. Commun.* 14 (2012) 86–89.
- [5] K. Chihara, A. Kitajou, I.D. Gocheva, S. Okada, J.-i. Yamaki, *J. Power Sources* 227 (2013) 80–85, <http://dx.doi.org/10.1016/j.jpowsour.2012.10.034>.
- [6] R.K.B. Gover, A. Bryan, P. Burns, J. Barker, *Solid State Ionics* 177 (2006) 1495–1500.
- [7] F. Sauvage, E. Quarez, J. Tarascon, E. Baudrin, *Solid State Sci.* 8 (2006) 1215–1221.
- [8] P. Serras, V. Palomares, A. Goñi, I. Gil de Muro, P. Kubiak, L. Lezama, T. Rojo, *J. Mater. Chem.* 22 (2012) 22301–22308.
- [9] S. Panero, B. Scrosati, M. Wachtler, F. Croce, *J. Power Sources* 129 (2004) 90–95.
- [10] M. Wagemaker, W.J.H. Borghols, F.M. Mulder, *J. Am. Chem. Soc.* 129 (2007) 4323–4327.
- [11] P. Poizot, S. Laruelle, S. Gruegeon, L. Dupont, J.-M. Tarascon, *Nature* 407 (2000) 496–499.
- [12] F. Badway, I. Plitz, S. Gruegeon, S. Laruelle, M. Dolle, A.S. Gozdz, J.-M. Tarascon, *Electrochim. Solid-State Lett.* 5 (2002) A115–A118.
- [13] P.G. Bruce, *Solid State Ionics* 179 (2008) 752–760.
- [14] Y. Ren, A.R. Armstrong, F. Jiao, P.G. Bruce, *J. Am. Chem. Soc.* 132 (2010) 996–1004.
- [15] P. Kubiak, T. Fröschl, N. Hüsing, U. Hörmann, U. Kaiser, R. Schiller, C.K. Weiss, K. Landfester, M. Wohlfahrt-Mehrens, *Small* 7 (2011) 1690–1696.
- [16] A. Tsirlin, R. Nath, A. Abakumov, Y. Fukurawa, D. Johnston, M. Hemmida, H.-A. Krug von Nidda, A. Loidl, C. Geibel, H. Rosner, *Phys. Rev. B: Condens. Matter Mater. Phys.* 84 (2011) 014429.
- [17] J.-M. Le Meins, M.-P. Crosnier-Lopez, A. Hemon-Ribaud, G. Courbion, *J. Solid State Chem.* 148 (1999) 260–277.
- [18] R.A. Shakoob, Dong-Hwa Seo, Hyungsuk Kim, Young-Uk Park, Jongsoon Kim, Sung-Wook Kim, Hyeokjo Gwon, Seongsu Lee, Kisuk Kang, *J. Mater. Chem.* 22 (2012) 20535–20541, <http://dx.doi.org/10.1039/c2jm33862a>.
- [19] S. Brunauer, P. Emmett, E. Teller, *J. Am. Chem. Soc.* 60 (1938) 309–319.